

The influence of a drag-reducing surfactant on a turbulent velocity field

By MICHAEL D. WARHOLIC, GAVIN M. SCHMIDT
AND THOMAS J. HANRATTY†

Department of Chemical Engineering, University of Illinois, Urbana IL 61801, USA

(Received 28 August 1997 and in revised form 7 December 1998)

A two-component laser-Doppler velocimeter, with high spatial and temporal resolution, was used to study how the introduction of a drag-reducing surfactant to water changes the fully-developed velocity field in an enclosed rectangular channel. Measurements were made for four different Reynolds numbers, $Re = 13\,300$, $19\,100$, $32\,000$, and $49\,100$ (based on the bulk viscosity, the half-height of the channel, and the viscosity of water). For a fixed volumetric flow the pressure drop was reduced by 62 to 76% when compared to a Newtonian flow with an equal wall viscosity. Measurements were made of the mean streamwise velocity, the root mean square of two components of the fluctuating velocity, the Reynolds shear stress and the spectral density function of the fluctuating velocity in the streamwise direction. The Reynolds shear stress is found to be zero over the whole channel and the spectra of the streamwise velocity fluctuations show a sharp cutoff at a critical frequency, f_c . The ratio of the cutoff frequency to the root mean square of the streamwise velocity fluctuations is found to be approximately equal to 1 mm^{-1} . The observation of a zero Reynolds shear stress indicates the existence of additional mean shear stresses (or mean transfers of momentum) that are not seen with a Newtonian fluid. Furthermore, the presence of a random fluctuating velocity field suggests a production of turbulence by a mechanism other than that usually found for a fully developed flow. Possible explanations for this behaviour are presented.

1. Introduction

Solutions of surfactants with high enough concentrations form aggregates that are called micelles. These were observed to cause drag reduction in turbulent flows of gasoline (Mysels 1949) and of water (White 1967). Studies of this phenomenon have been summarized by Ohlendorf, Inthertal & Hoffman (1986), Zakin & Lui (1983), and Gyr & Bewersdorff (1995). A remarkable observation is that drag reduction approaching 80% can be realized when the composition is such that rod-like micelles are formed (Ohlendorf *et al.* 1986). This paper presents measurements of turbulence properties of a solution of tris-hydroxyethyl-ammonium acetate (Ethoquad T/13-50) and sodium salicylate (NaSal) flowing in a $5.08\text{ cm} \times 61.0\text{ cm}$ rectangular channel. The make-up of the solution used in the experiments was suggested by J. L. Zakin and B. Lui (Ohio State University) as yielding very large reductions in drag. The system was turbulent flow in a $5.08\text{ cm} \times 61.0\text{ cm}$ rectangular channel. Four Reynolds numbers were studied, $Re = 13\,300$, $19\,100$, $32\,000$ and $49\,100$. Here, the Reynolds number is defined in terms of the half-height of the channel, the bulk velocity, and the viscosity of water.

† Author to whom correspondence should be addressed: e-mail: thanratt@uiuc.edu.

Measurements of the root mean square of the streamwise and wall normal velocity fluctuations and of the Reynolds shear stress have been reported by Kawaguchi *et al.* (1996). They used a 4 cm \times 50 cm rectangular channel and a solution of cetyltrimethylammonium chloride (CTAC) and NaSal. Measurements of Povkh, Stupvi & Aslanov (1988) of the root mean square of the streamwise and wall normal velocity fluctuations and of the Reynolds shear stress for a solution of *n*-hexadecyltrimethylammonium bromide (C₁₆TABr) and NaSal flowing in a square (15 mm) channel are described by Gyr & Bewersdorff (1995). Studies of axial velocity fluctuations with solutions of C₁₄TABr and NaSal and of C₁₆TABr and NaSal flowing in a pipe with a diameter of 5 cm at $Re = 35\,000$ and $120\,000$ have been carried out by Bewersdorff & Ohlendorf (1988). Streamwise and spanwise fluctuations have been measured by Chara *et al.* (1993), in a 3.94 cm pipe, with the surfactant Habon G, manufactured by Hoechst Company. It consists of 53.5 wt% active surfactant, 10.2 wt% isopropanol and 36.3 wt% water. The cation of the surfactant was hexadecyldimethylhydroxyethylammonium and the counter ion was 3-hydroxy-2 naphthoate. Gyr & Bewersdorff also discuss results obtained by Beiersdorfer, Bewersdorff & Gyr (1994), with the same micelle system as used by Bewersdorff & Ohlendorf, in a square channel (15 mm).

The measurements of Povkh *et al.* (1988) show that the maximum in the intensity of the streamwise velocity fluctuations is shifted farther away from the wall with increasing drag-reduction. The intensity of the turbulent velocity component normal to the wall was found to be reduced by about 50%. Gyr & Bewersdorff (1995) present one figure from the study of Beiersdorfer *et al.* (1994) that shows a value of the Reynolds stress that is close to zero over the whole channel cross-section. Gyr & Bewersdorff (1995) also report, for flow in both a channel and a pipe, that the sum of the Reynolds stress and the viscous stress (calculated with the viscosity at low shear rates or with the solvent viscosity) may not be equal to the stresses calculated from measurements of the pressure gradient. They suggest that this stress deficit could be due to an increase in the shear viscosity (Bewersdorff 1990).

Kawaguchi *et al.* (1996) presented turbulence measurements obtained at a Reynolds number of 5072 (based on the solvent viscosity and the half-height of the channel). The drag-reduction was of the order of 75%; the measured velocity fluctuations normal to the wall were greatly reduced and the measured Reynolds shear stress was close to zero. These results are of particular interest because results have recently been obtained in our laboratory (Schmidt 1997; Warholic 1997) which also show zero Reynolds shear stresses. The works of Schmidt (1997) and Warholic (1997), reported in this paper, were carried out with a wider range of Reynolds numbers and with a different surfactant system to that used by Kawaguchi *et al.* and by Beiersdorfer *et al.* Reynolds stresses were found to be close to zero at all Reynolds numbers. Viscometric measurements show that the velocity profile cannot be explained by using the laminar flow relation for a shear thinning fluid. Spectral measurements reveal a sharp cutoff of velocity fluctuations at large frequencies.

A remarkable feature of results for surfactant solutions with large drag-reduction is that turbulence is not produced by the classical method, observed for fully developed flow of a Newtonian fluid. Furthermore, a consideration of the mean velocity profiles suggests the existence of mean shear stresses that are not observed in rheological studies. A possible explanation is that time-averaged and fluctuating stresses, that are not present under steady flow conditions, are introduced by the interaction of turbulence with the micelles. Conservation of mechanical energy then suggests that fluctuating micelle stresses supply energy to the fluctuating fluid velocities.

2. Mechanical energy balance

For a fully developed two-dimensional flow, with the mean velocity defined as $U(y)$, the balance of mean kinetic energy gives

$$0 = -\frac{U}{\rho} \frac{dP}{dx} + \frac{d}{dy} \left(\frac{U T_{yx}}{\rho} - \overline{vu}U \right) + \overline{uw} \frac{dU}{dy} - \frac{T_{xy}}{\rho} \frac{dU}{dy}, \quad (1)$$

where u and v are the fluctuating velocity components in the x - and y -directions, P , the mean pressure, T_{xy} , the mean shear stress and ρ , the density. A balance of the mean turbulent kinetic energy, $\frac{1}{2}\overline{q^2}$, gives

$$0 = \frac{d}{dy} \left[-v \left(\frac{p}{\rho} + \frac{q^2}{2} \right) + \frac{\overline{u_i \tau_{yi}}}{\rho} \right] - \overline{uw} \frac{dU}{dy} - \frac{\overline{\tau_{ij} \partial u_j}}{\rho \partial x_i}, \quad (2)$$

where τ_{ij} is a fluctuation in the stress, $q^2 = u^2 + v^2 + w^2$, repeating indices indicate a summation, and p is a fluctuating pressure.

An average of (1) and (2) over the channel cross-section gives

$$0 = -\frac{\langle U \rangle}{\rho} \frac{dP}{dx} - \left\langle \frac{T_{xy}}{\rho} \frac{dU}{dy} \right\rangle + \left\langle \overline{uw} \frac{dU}{dy} \right\rangle, \quad (3)$$

$$0 = -\left\langle \overline{uw} \frac{dU}{dy} \right\rangle - \left\langle \frac{\overline{\tau_{ij} \partial u_j}}{\rho \partial x_i} \right\rangle. \quad (4)$$

For an incompressible Newtonian fluid

$$T_{xy} = \mu \left(\frac{dU}{dy} \right), \quad (5)$$

$$\tau_{ij} = \mu \left(\frac{\partial u_i}{\partial x_j} + \frac{\partial u_j}{\partial x_i} \right). \quad (6)$$

Both $\bar{\epsilon} = \langle T_{xy}(dU/dy) \rangle$ and $\epsilon' = \langle \overline{\tau_{ij}(\partial u_j/\partial x_i)} \rangle$ are positive. They, respectively, represent the direct dissipation of the mean flow energy by viscosity and the dissipation of energy associated with the fluctuating velocity field. Equation (3) indicates that the energy input by the pressure gradient is directly dissipated by viscosity and is used to produce velocity fluctuations through the term $\langle -\overline{uw}(dU/dy) \rangle$. Equations (4) and (6), for a Newtonian fluid, show that the energy transferred into velocity fluctuations is dissipated by viscosity. If the Reynolds stress is zero, turbulence cannot be created.

Experimental results on the flow of solutions of micelles show that, in an unsteady three-dimensional field, stresses can arise which are not observed in steady rheological flows. This behaviour is interpreted as resulting from the time-varying configurations of the micelles; it is represented by added stresses. Thus,

$$T_{ij} = T_{ij}^v + T_{ij}^m, \quad (7)$$

$$\tau_{ij} = \tau_{ij}^v + \tau_{ij}^m, \quad (8)$$

where T_{ij}^v and τ_{ij}^v are defined by equations of the form of (5) and (6) and the viscosity is obtained from rheological experiments. Stresses T_{ij}^m and τ_{ij}^m are the mean and fluctuating part of the added stress.

Equations (3) and (4) then become

$$0 = -\frac{\langle U \rangle}{\rho} \frac{dP}{dx} - \left\langle \frac{1}{\rho} T_{xy}^v \frac{dU}{dy} \right\rangle - \left\langle \frac{1}{\rho} T_{xy}^m \frac{dU}{dy} \right\rangle + \left\langle \overline{uw} \frac{dU}{dy} \right\rangle, \quad (9)$$

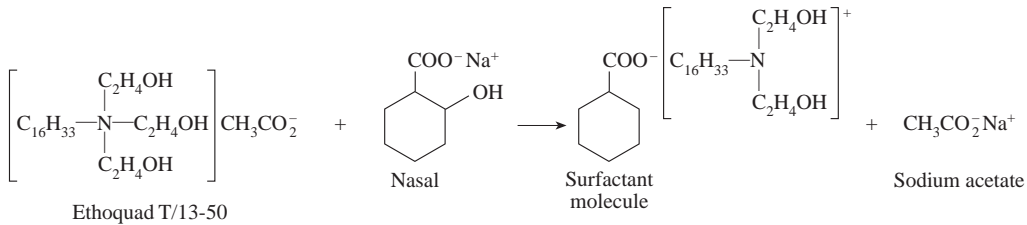
$$0 = - \left\langle -\bar{u}\bar{v} \frac{dU}{dy} \right\rangle - \left\langle \frac{\tau_{ij}^v \partial u_j}{\rho \partial x_i} \right\rangle - \left\langle \frac{\tau_{ij}^m \partial u_j}{\rho \partial x_i} \right\rangle. \quad (10)$$

The second term, ϵ^v , is always positive. However, the added stress, τ_{ij}^m , need not be related to the rate of strain through equations such as (5) and (6). Actually, it could be a function of all the components of rate of strain tensor and not just $(\partial u_i / \partial x_j + \partial u_j / \partial x_i)$. Consequently, the third term, ϵ^m , could be plus or minus. A minus value results in a production of velocity fluctuations.

3. Description of experiments

3.1. Surfactant solution

A surfactant molecule has a hydrophilic head and a hydrophobic tail. The negatively charged head group acts as a counter ion to the positively charged tail. When surfactant molecules are added to a protic solvent, such as water, the hydrophilic ends are repulsed by the positively charged environment. If the surfactant molecules are present in an amount larger than the critical micelle concentration (CMC), an energetically favourable aggregate occurs. The surfactant molecules come together in a ball shape with the hydrophilic head groups forming a shell around the hydrophobic tails. However, the hydrophobic core is not completely insulated from the outside water since the head groups repel one another (as they have the same charge). By altering the environment, the repulsion of the head groups can be reduced so that rod-shaped micelles form at a concentration, c_t , which is larger than CMC. The presence of electrolytes in the solution buffers the charges of the head groups and allows them to pack closer together. This reduces the magnitude of c_t . Consequently, tap water is more beneficial than deionized water in promoting the sphere to rod transition. The choice of the counter ion also affects the tendency to form rods. Less soluble counter ions bind strongly to the micelle interface and increase the stability of the rods. The increase in surfactant concentration beyond CMC favours rod formation, since this geometry allows more micelles to pack together in a given volume. A decrease in temperature is associated with a decrease in the length of the rods and, therefore, a decrease in drag-reduction. A solution of Ethoquad T/13-50 (obtained from Akzo Chemicals) and sodium salicylate was used. Zakin suggested an optimal ratio of 12 moles of NaSal to 5 moles of Ethoquad T/13-50 and a composition of about 2000 p.p.m. of Ethoquad T/13-50. The Ethoquad T/13-50 arrived as a pungent, thick, brown liquid with a composition of 50 wt% of active surfactant, 36 wt% isopropanol and 14 wt% water. The molecular weights of the Ethoquad T/13-50 and the sodium salicylate are, respectively, 454 g mol^{-1} and $160.11 \text{ g mol}^{-1}$. The reaction that occurs is given in scheme 1.



Scheme 1.

The flow facility was not completely filled with tap water so that sufficient empty

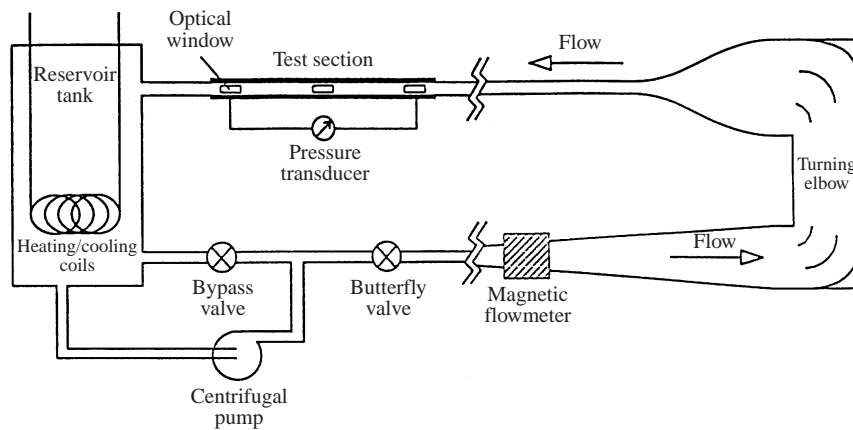


FIGURE 1. Diagram of the flow facility.

space existed in the reservoir tanks to add the chemicals. The Ethoquad T/13-50 and NaSal were dissolved separately before being added to the channel. Approximately 8.8 kg of NaSal was dissolved in tap water at room temperature in a stirred tank. This solution was then pumped directly into the reservoir tank. Approximately 5.7 gallons of Ethoquad T/13-50 was mixed with tap water at room temperature to produce a solution with a tinge of brown colour. Large amounts of foam were produced when this was pumped into the channel. The amount of foam decreased significantly after circulating in the flow loop for several hours. Experiments were carried out for two days while the solution in the channel remained clear. The experiments were discontinued on the third day because the solution took on a milky appearance. A new solution was then made up. Results obtained at the end of a run were the same as at the beginning. The main reason for changing the solution was that the optical quality of the signals deteriorated.

3.2. The flow facility

The flow facility used in the experiments is depicted in figure 1. Details of its design and the optical measurements are given by Niederschulte, Adrian & Hanratty (1990) Günther *et al.* (1998) and Warholic (1997). The liquid was circulated with the smaller of the two centrifugal pumps. The reservoir contained cooling coils that maintained the temperature at 25 °C. The total volume of the system was 1370 gallons.

The rectangular channel had a length of 11 m and was constructed of stainless steel. Velocity measurements were made in the final 3 m, where a number of previous studies with Newtonian fluids have revealed that the flow is fully developed. For example, measurements of mean velocity profiles and Reynolds stresses are found to agree very closely with direct numerical simulations of flow in a two-dimensional channel at $Re = 2777$ and 2456 (Niederschulte *et al.* 1990) and at $Re = 5700$ (Günther *et al.* 1998). Optical grade glass windows allowed the insertion of laser light on one side and the collection of scattered light on the opposite side. The pressure gradient was measured with pressure taps located on the bottom wall of the channel and separated by a distance of 152 cm. A Validyne Variable Reluctance Pressure Transducer (Model DP103) was used.

3.3. Velocity measurements

The velocity field was measured with a three-beam, two-colour LDV system manufactured by TSI. A beam expanding module (TSI Model 9832) and a forward scattering

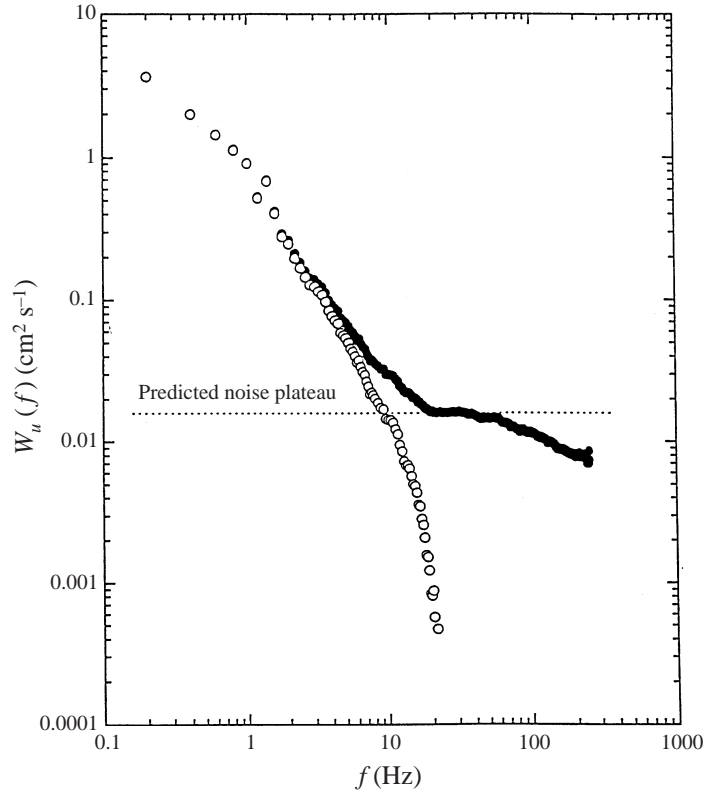


FIGURE 2. ●, Raw and ○, corrected streamwise spectra at $y/H = 0.6$ for $Re = 19\,100$.

mode were used. The measuring volume had a diameter of $45\ \mu\text{m}$ and a length of $0.44\ \text{mm}$. The fluid was seeded with $700\ \text{nm}$ polystyrene spheres. The number was controlled so that, on average, only one particle passed through the measuring volume at given time.

The signals were corrected for white noise by considering the frequency spectra. This is illustrated in figure 2, which shows the spectral density function that was measured with the surfactant solution at $Re = 19\,100$. The value in the plateau is subtracted from the measured spectral energy at all frequencies to determine a corrected spectrum, which is then integrated to determine the mean square of the turbulent velocity fluctuations. The damping of the high-frequency velocity fluctuations by the surfactant solutions produced spectra whose range of frequencies were compatible with the sampling rate, even at the highest Reynolds number. Thus, the method of correction was more easily implemented than with water flows.

Details regarding the measuring methods and the noise correction are contained in a recent article by Günther *et al.* (1998).

4. Results

4.1. Rheological measurements

The rheological behaviour of the Ethoquad T/13-50 solution (2000 p.p.m.) was investigated in a Bohlin CS (constant stress) rheometer with a double gap Couette geometry. The gap width used was $2.25\ \text{mm}$. A constant shear stress was applied to

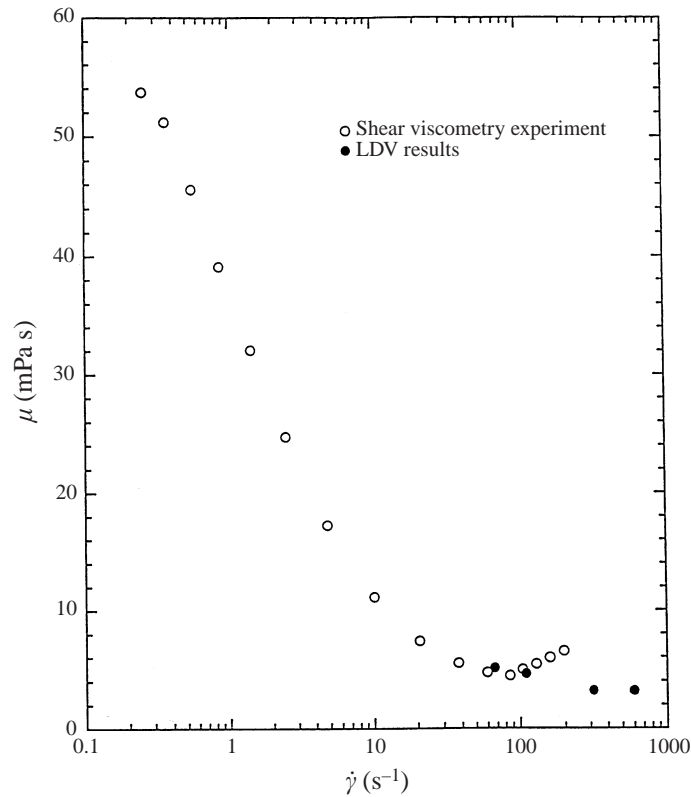


FIGURE 3. Shear viscosity, μ , as a function of the shear rate, $\dot{\gamma}$.

the solution and the resulting shear rate was measured over a preset time. These measurements were performed at 25°C, the same temperature that was used for the LDV measurements. The open circles in figure 3 present the viscosity as a function of shear rate. The Ethoquad T/13-50 shows a shear thinning behaviour out to a shear rate of 100 s^{-1} . The rise in viscosity beyond $\dot{\gamma} = 100\text{ s}^{-1}$ is attributed to a Taylor instability, which is known to occur in the instrument at this shear rate.

The measurements of the mean velocity profiles in the experiments in the channel gave shear rates at the wall of 67, 117, 321 and 588 s^{-1} . Pressure drop measurements and the assumption of a fully developed flow were used to calculate the shear stress at the wall.

Viscosities calculated from the ratio of T_w and $(dU/dy)_w$ give the viscosities in table 1; these are plotted as filled points in figure 3. These data show a slight shear thinning; they overlap nicely with the measurements obtained with the rheometer. An important aspect of these results is that no sudden increase in viscosity is observed over the range of $\dot{\gamma}$ characterizing the experiments.

Extensive studies of the rheological behaviour of Ethoquad with different amounts of NaSal have been made by Hoffman, Stern & Myska (1994) and by Lui, Yeshayahu & Zakin (1996). Shear thinning was observed at molar ratios of NaSal to Ethoquad in the range used in this study. Hoffman *et al.* have interpreted this shear thinning as indicating the formation of 'weak network structures'. Cryo-TEM pictures of these structures, obtained by Lui *et al.*, confirm the existence of thread-like micelles as

Solution	Re^\dagger	$\frac{\Delta P}{\Delta x}$ (dynes cm ⁻³)	T_w (dynes cm ⁻²)	u^* (cm s ⁻¹)	$\left(\frac{dU}{dy}\right)_{wall}$ (s ⁻¹)	μ_{wall} (g cm s ⁻¹)
Ethoquad T/13-50	13 300	1.46	3.42	1.85	67	5.1
water	14 300	2.79	6.56	2.56	—	0.9
Ethoquad T/13-50	19 100	2.29	5.37	2.32	117	4.6
water	20 300	5.17	12.1	3.48	—	0.9
Ethoquad T/13-50	32 000	4.37	10.26	3.20	321	3.2
water	31 200	—	26.00	5.10	—	0.9
Ethoquad T/13-50	49 100	8.01	18.82	4.34	588	3.2
water	48 800	—	59.60	7.72	—	0.9

TABLE 1. Summary of pressure drop measurements.

well as an entanglement network. Normal stress and dynamic viscosity measurements indicate that the solution used in this study is viscoelastic.

A sharp increase in the viscosity of the order of 40–50% was noted at $\dot{\gamma} \cong 500 \text{ s}^{-1}$ by Hoffman *et al.* and at $\dot{\gamma} \cong 200 \text{ s}^{-1}$ by Lui *et al.* Both groups interpret this jump as indicating the formation of shear-induced structures, identified by a number of investigators (Ohlendorf *et al.* 1986). These SIS are described by Hoffman *et al.* as follows: ‘The characteristic feature of viscoelasticity is the smoothly increasing orientation of the micellar network structures toward the direction of flow while the transition into SIS is marked by a sudden switch into a state of complete alignment’.

The measurements shown in figure 3 give no evidence of a transition to an SIS in the range of $\dot{\gamma}_w$ of 67–588 s⁻¹, characterizing the experiments. This could indicate that turbulence inhibits their formation. However, a more likely explanation is that a temperature of 25 °C was used in the experiments; Hoffman *et al.* and Lui *et al.* carried out their experiments at 20 °C.

The conclusions from these studies is that the solution used in the experiments described in this paper is shear thinning and viscoelastic; the micelles assume thread-like structures which can form a network.

4.2. Measurements of the pressure drop

The average wall shear stresses, for the Ethoquad T/13-50 and pure water, at each Reynolds number was determined from measurements of the pressure drop, by using a force balance across the test section:

$$T_w = H \left(\frac{\Delta P}{\Delta x} \right)_{measured}, \quad (11)$$

where H is the half channel height. Table 1 summarizes the results.

This method for determining the wall shear stress was tested in studies with water by measuring the total shear stress, equal to the sum of the Reynolds stress and the viscous mean stress, at different locations (Warholic 1997). Extrapolations of these results to the wall gave a value for T_w that agrees with that calculated from (11).

A number of studies of water flows in the channel have given the following relations for the wall stress:

$$C_f = T_w / \frac{1}{2} \rho U_B^2, \quad (12)$$

Re^*	%DR \dagger	$Re\ddagger$	Calculated $\Delta P/\Delta x$ (dynes cm $^{-2}$)	%DR \S
13 300	48	2310	8.9	62
19 100	56	3690	16.3	67
32 000	61	8880	36.8	72
49 100	68	13 650	78.0	76

* Re is based on the viscosity of water.

\dagger DR compared to water.

\ddagger Re is based on the wall viscosity for the Ethoquad T/13-50 runs.

\S DR compared to a Newtonian fluid with the wall viscosity.

TABLE 2. Summary of percentage drag reduction.

$$C_f = 0.073 \left(\frac{2HU_B\rho}{\mu} \right)^{-0.25}, \quad (13)$$

where U_B is the integrated average velocity in the central regions of the test section. The measured wall shear stress for the Ethoquad solution can be compared to the wall shear stress for a Newtonian fluid with the equation

$$\%DR = \frac{T_{w,Newtonian} - T_{w,Ethoquad}}{T_{w,Newtonian}} \times 100. \quad (14)$$

Table 2 summarizes results from (14) for two reference conditions. In one of these, $T_{w,Newtonian}$ is calculated from (12) and (13) using the viscosity of water. In the other, $T_{w,Newtonian}$ is calculated using the viscosity of the Ethoquad solution at the wall. The percentage drag-reduction is seen to increase with increasing Reynolds number. For definition 1, it is 48% at $Re = 13\,300$ and 68% at $Re = 49\,100$. Using definition 2, the drag reduction changes from 76% at $Re = 49\,100$ to 62% at $Re = 13\,300$.

4.3. LDV measurements

Figure 4 shows the average streamwise velocity versus distance from the wall. The ordinate has units of cm s^{-1} and the abscissa is made dimensionless with the half-height of the channel. Measurements for water at approximately the same volumetric flowrate are also presented. As has been noted in several previous studies (Bewersdorff & Ohlendorf 1988; Zakin, Myska & Chara 1996), the velocity profiles of surfactant solutions are more diffuse than those for water, suggesting a closeness to laminar flow.

Because of the size of the measuring volume ($40\,\mu\text{m}$) and of noise due to light reflections, average velocities could not be measured any closer to the wall than $0.16\,\text{mm}$. For water flows, this was too large to determine the shearing rate at the wall directly. However, for flows with surfactant solutions, this was not the case. The values of $(dU/dy)_{wall}$ given in table 1 were obtained by fitting measurements of U close to the wall where the shear stress is approximately constant, with a straight line (see figure 4). The same results could also be obtained by using a parabolic fit (see figure 9). The shear rate at the wall was not used to determine T_w in any of these measurements because of uncertainties in defining the viscosity of the surfactant solution. The values of μ_{wall} given in table 1 were obtained by dividing measured values of T_w and $(dU/dy)_{wall}$.

Measurements of the mean velocity are plotted in semi-logarithmic coordinates in figure 5. The velocities are made dimensionless with the measured friction velocities

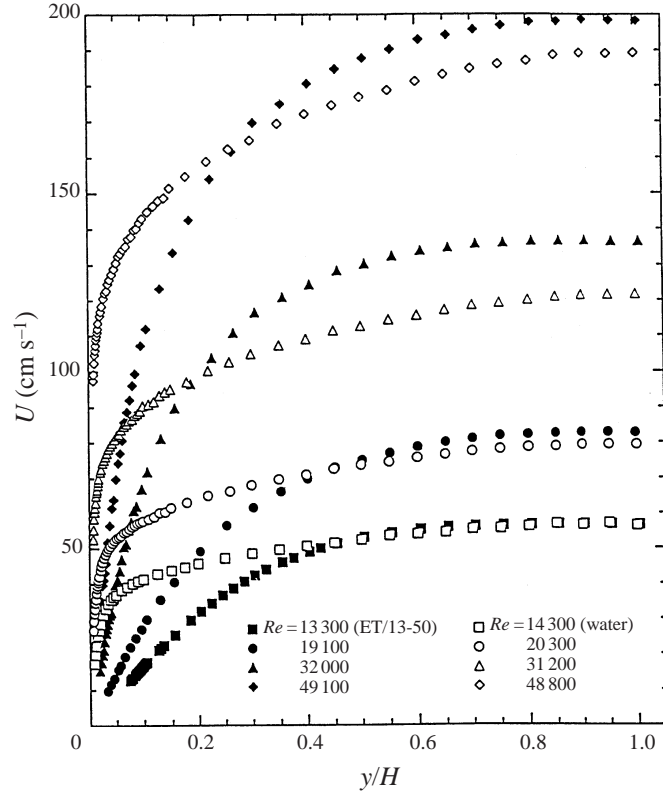


FIGURE 4. Mean streamwise velocity, U , versus normalized distance from the wall, y/H .

in table 1. The distances from the wall are made dimensionless with viscous lengths defined as the ratio of the measured wall viscosity to the friction velocity. The solid line is Virk & Mickley's (1970) asymptote for maximum drag-reduction,

$$U^+ = 11.7 \ln(y^+) - 17.0. \quad (15)$$

For $15 < y^+ < 30$ the non-dimensional velocity profiles are close to Virk & Mickley's asymptote. For $y^+ > 30$, the profiles initially exceed Virk & Mickley's asymptote. They drop below the asymptote in the centre of the channel. The behaviour in figures 4 and 5 suggests that the mean velocity profile can be described by a laminar relation for a significant region close to the wall, particularly if shear thinning is assumed. This matter is explored further in figure 9.

Figures 6 and 7 present root mean squares of the streamwise and normal velocity fluctuations, made dimensionless with the measured friction velocities. Results for Ethoquad T/13-50 at $Re = 13\,300$ are not included because the noise level was too large. At $Re = 32\,000$ and $49\,100$ the maximum in the measured u'^+ is larger than would be observed for water flowing at the same volumetric flowrate; at $Re = 19\,100$ the maximum u'^+ is much smaller than that observed for water. The location of the maximum u'^+ is farther away from the wall, at all three Reynolds numbers, than that found for water. The maximum v'^+ is drastically decreased, when compared to water measurements at the same volumetric flowrates. Similar results for u'^+ and v'^+ have been observed in turbulence measurements with other surfactant solutions. However, differences are noted which probably reflect differences in the rheological behaviour.

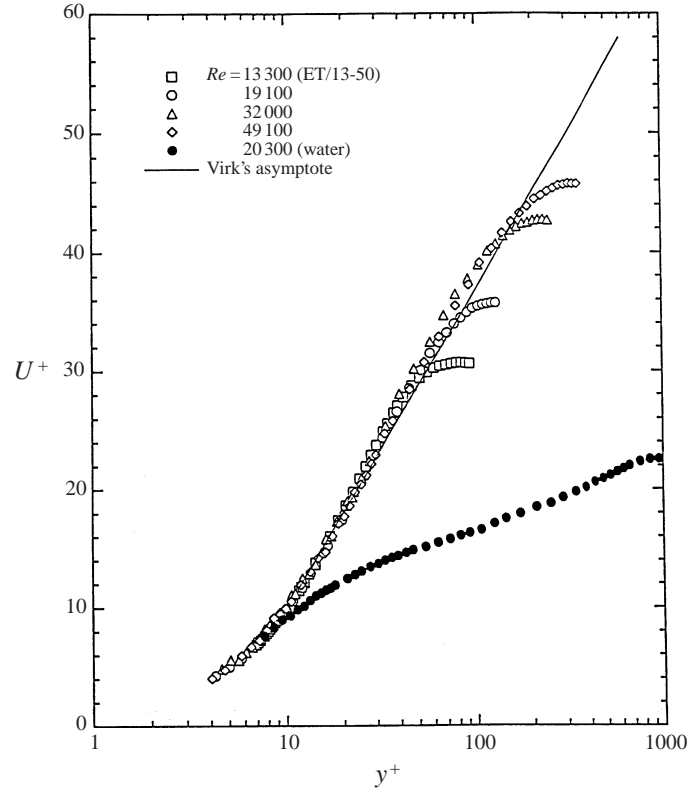


FIGURE 5. Comparison of non-dimensional velocity profiles for 2000 p.p.m. Ethoquad T/13-50 solutions at the four Reynolds numbers studied to a typical Newtonian profile.

Measured Reynolds stresses are plotted in figure 8. The Reynolds stress is found to be close to zero for the surfactant solution over the entire channel cross-section for all three Reynolds numbers.

Theoretical laminar velocity profiles can be calculated from the equation,

$$U = \frac{H}{T_w} \int_T^{T_w} \frac{T}{\mu} dT. \quad (16)$$

Two cases were investigated. For a constant viscosity fluid,

$$U = \frac{T_w}{2\mu_w} \left\{ 2y - \frac{y^2}{H} \right\}, \quad (17)$$

where y is the distance from the channel wall and μ_w is the measured wall viscosity. For a variable viscosity, equation (16) is integrated using the viscosities given in figure 3. The theoretical laminar profiles are compared with measurements for $Re = 19100$ in figure 9. The measured profile agrees with the laminar relation out to $y/H \simeq 0.2$. For $y/H > 0.2$, the laminar profiles show a greater slope than the measurements. Similar results are obtained for the other two Reynolds numbers.

The poor agreement in figure 9 suggests the presence of an additional stress, which we interpret as being caused by the interaction of the turbulence with the micelles.

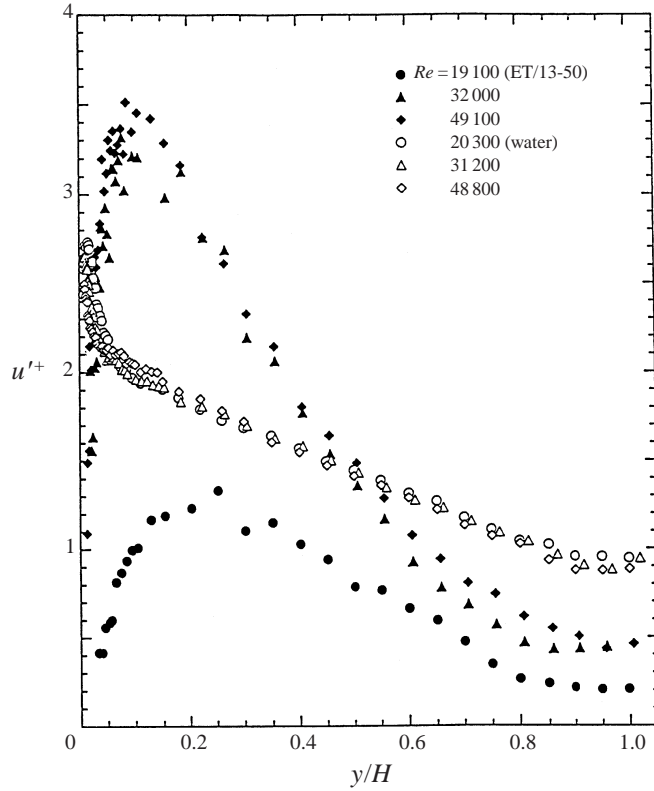


FIGURE 6. Non-dimensional streamwise turbulence intensities, u'^+ , versus the normalized distance from the wall, y/H .

Thus,

$$T^t = T^v + T^r + T^m, \quad (18)$$

where T^t is the total shear stress, T^v , the viscous shear stress, T^r , the Reynolds shear stress, and, T^m , the additional stress. Figure 10 presents measured values of T^m , obtained from (18), along with the total stresses for each Reynolds number. The behaviour is the same for all Reynolds numbers. The micelle shear stress is zero in the region where the velocity is varying linearly with distance from the wall. It increases to a maximum and then decreases linearly to zero at the centre of the channel.

Power spectra of the streamwise velocity fluctuations at four different y -locations for the Ethoquad T/13-50 and for water are compared in figure 11. The spectral density functions are normalized by the mean square of the velocity fluctuations so that the area under each curve is equal to unity. The addition of the surfactant increases the importance of contributions at low frequencies relative to those for high frequencies, for all Reynolds numbers and for all y -locations. This is consistent with LDV measurements made in the same facility with water solutions of drag-reducing polymer molecules (Warholic 1997). A feature in figure 11, not observed for water, is the sharp cutoff of the power density function above a certain frequency. The magnitude of this cutoff frequency varies with both the Reynolds number and the y -location. Figure 12 shows the power spectra of Ethoquad T/13-50 and of water at $y/H = 0.6$, with both the frequency and the spectral density function divided

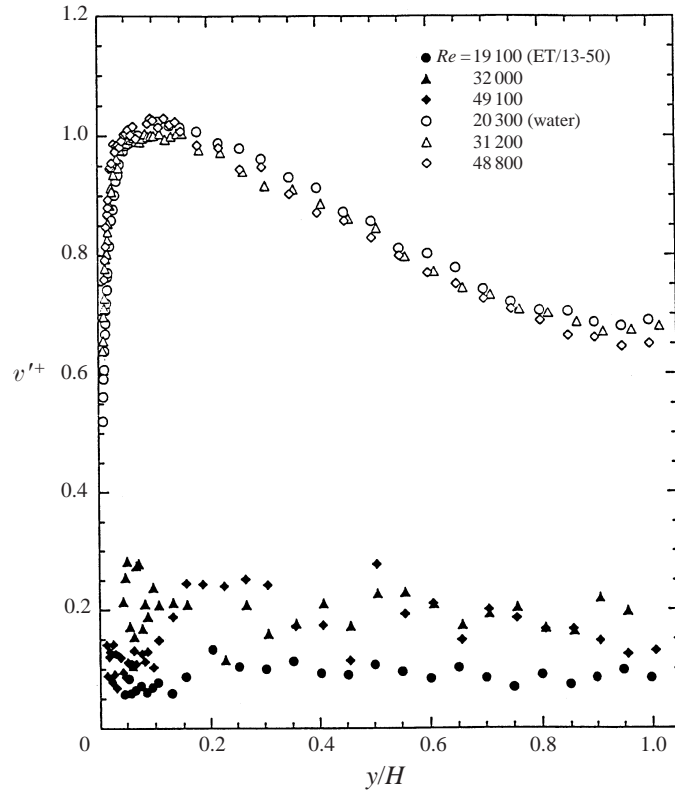


FIGURE 7. Non-dimensional normal turbulence intensities, v'^+ , versus the normalized distance from the wall, y/H .

by the inverse of the root mean square of the velocity fluctuations. When scaled in this manner, the cutoff frequency for the different Reynolds numbers agree (within the accuracy of the noise correction). Similar results are obtained for measurements at $y/H = 0.1, 0.4, 1.0$. In fact, there is a rough quantitative agreement of all of the measurements of spectral density functions when plotted in this way. These results suggest a critical value of the scaled frequency between 10 and 15 cm^{-1} , or a critical lengthscale for this surfactant system of the order of 1 mm .

5. Discussion

Solutions of surfactants in water can be formulated so that rod-shaped micelles are created. The presence of these micelles causes a large reduction in drag over what would be experienced with a Newtonian fluid flowing turbulently at the same rate. The system studied in this research was shown to be shear thinning, from measurements in a Couette viscometer and from measurements of the velocity gradient at the wall under turbulent flow conditions. The wall shear stress was reduced 62 to 76% from what would be realized by a Newtonian fluid with a viscosity equal to the value measured at the wall. It was reduced 48 to 68% when compared to water flowing at approximately the same rate.

The remarkable feature of micelle solutions with large amounts of drag-reduction

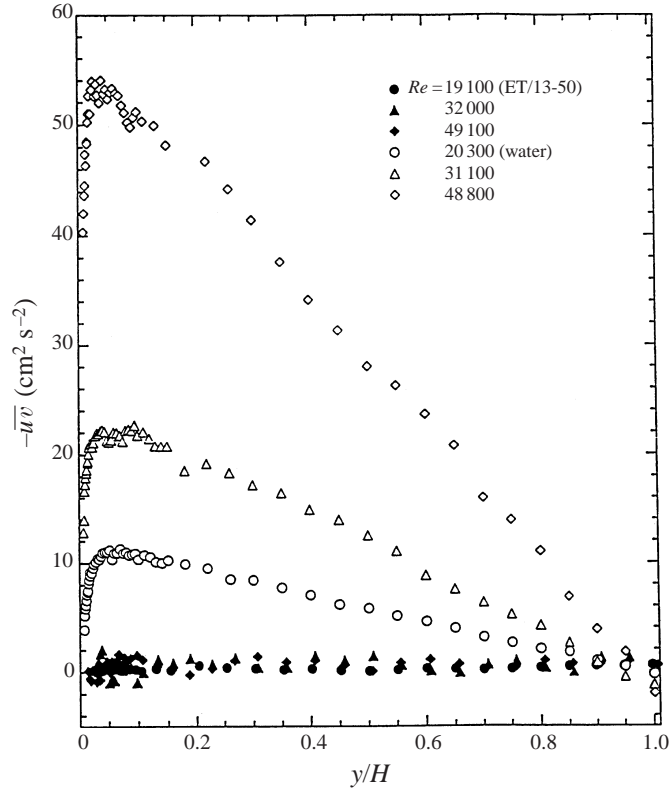


FIGURE 8. Mean Reynolds stress, \overline{uv} , versus normalized distance from the wall, y/H .

is that the Reynolds stresses are zero (within experimental error) over the entire cross-section of the channel and the mean velocity profile cannot be calculated from a laminar flow relation, using viscosity data obtained in a Couette viscometer. The absence of Reynolds shear stresses means that

$$-\overline{uv} \frac{dU}{dy} = 0, \quad (19)$$

so the classical method for producing turbulence by a fluid flowing parallel to a smooth boundary is absent. These observations raise two intriguing questions: How do we account for the added mean stress defined by (18)? How are the turbulent velocity fluctuations produced?

One possibility is that secondary flows exist in a channel. Then, an additional mean transport of momentum in the y -direction could occur. Since the flow would be three-dimensional, turbulence could be produced through terms such as $\overline{v^2}(\overline{dV}/dy)$, $(\overline{wv})(\overline{dW}/dy)$, $\overline{w^2}(\overline{dW}/dz)$, $\overline{vw}(\overline{dV}/dz)$. We have no direct proof that a significant secondary flow did not exist in the part of the channel in which turbulence measurements were made. However, there are a number of reasons to rule this out as an explanation for the results. Measurements with a Newtonian fluid have shown no evidence of secondary flows and agree with direct numerical simulations (Niederschulte *et al.* 1990; Günther *et al.* 1999). Studies, with particle image velocimetry of flows of solutions of drag-reducing polymers in the same equipment, do not show a secondary flow,

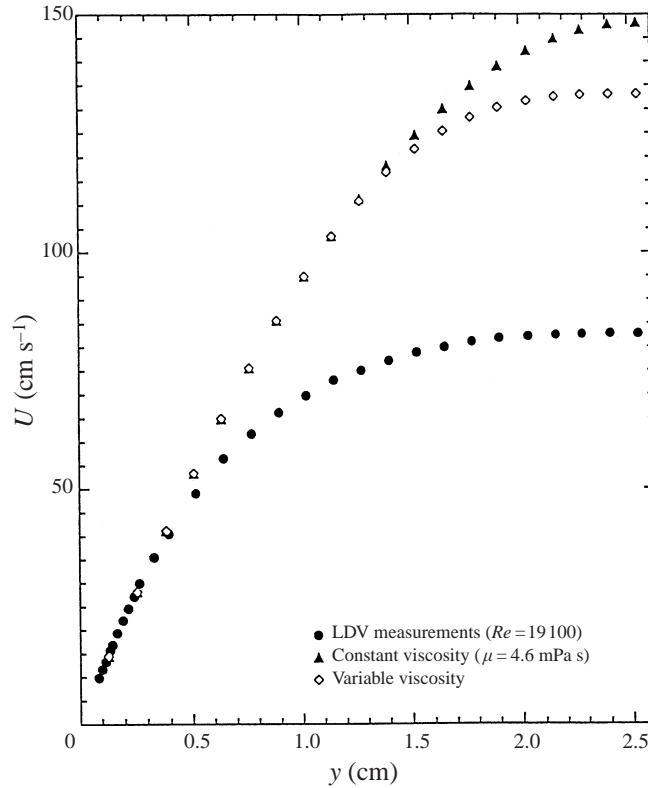


FIGURE 9. Measured mean streamwise velocities at $Re = 19\,100$ compared to theoretical laminar velocity profiles.

even under conditions close to maximum drag-reduction (Warholic 1997). Added stresses and turbulent velocity fluctuations have been found under conditions close to maximum drag-reduction with flows in circular pipes for which secondary flows should not exist (Bewersdorff & Ohlendorf 1985).

If the flow is fully-developed and two-dimensional, equations (9) and (10) are valid. The interpretation of these equations is straightforward for polymer solutions, for which maximum drag-reduction can be realized with polymer concentrations as low as 5 p.p.m. The stresses T_{ij}^v and τ_{ij}^v are then defined with Newton's law of viscosity and a constant viscosity equal to that of the solvent. Surfactant solutions are more complicated since they are shear-thinning.

The approach outlined in §2 is to define T_{ij}^v and τ_{ij}^v with equations (5) and (6) and to use a viscosity that is the function of the rate of strain determined from rheological measurements under conditions of steady flow. Then, $\langle \tau_{ij}^v(\partial u_j / \partial x_i) \rangle$ is a positive number. If the Reynolds stress is zero, equation (10) indicates that $\langle \tau_{ij}^m(\partial u_j / \partial x_i) \rangle$ must be negative for an unsteady flow to exist. Thus, a consideration of conservation of mechanical energy indicates that fluctuating stresses resulting from the interaction of fluid velocity fluctuations with the micelles can supply energy to the fluid.

A consideration of equation (9) for a zero Reynolds stress shows that there is an additional contribution to the pressure gradient in a turbulent flow from $T_{xy}^m(dU/dy)$. This term represents the additional mean flow energy needed to cause the micelles to

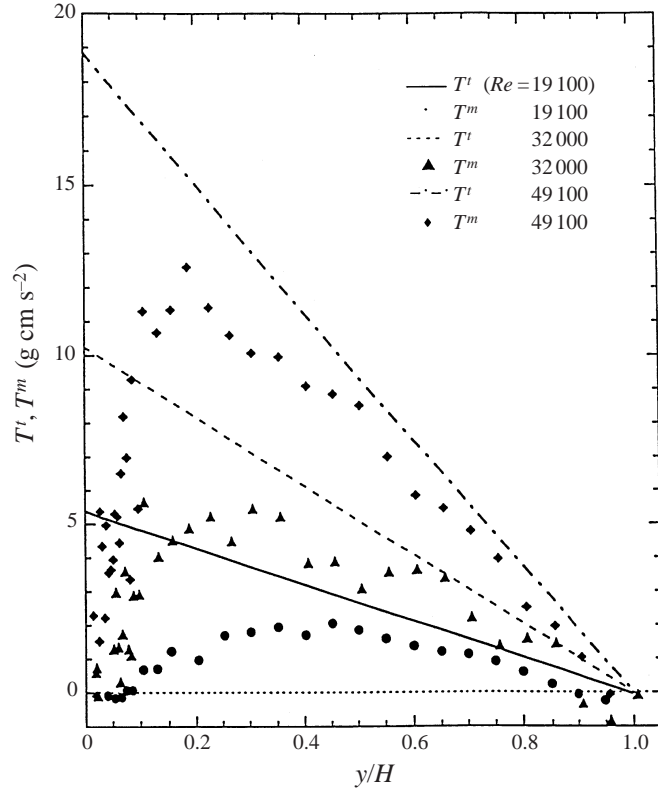


FIGURE 10. Shear stress contribution due to micelles, T^m , and total stress, T^t , versus normalized distance from the wall, y/H .

reorient as a result of the unsteady three-dimensional velocity field. In particular, they would have a time-changing and, possibly, a different time-mean configuration to that which exists in a steady flow with the same mean velocity gradient. This additional energy is eventually released to the fluid, through the term $\langle \tau_{ij}^m (\partial u_j / \partial x_i) \rangle$.

If, as suggested above, the turbulence production and the added shear stress depend on the properties of the surfactant solution, one should expect different systems to produce different velocity fields. This could explain why the profiles of average velocity measured by Zakin *et al.* (1996) differ from the results presented in this paper and why turbulence can be different for different surfactant systems, even when compared at the same percentage drag-reduction.

Another feature of the turbulence properties of solutions of micelles, not observed with Newtonian fluids, is a sharp drop-off of the spectral density function at a certain frequency, f_c . Both Bewersdorff & Ohlendorf (1988) and Hofmann *et al.* (1994) have shown that solutions containing micelles have elastic properties. It is reasonable to assume that the drop-off is related to an elastic time constant. However, it is not obvious how to connect this idea with the observation that f_c varies inversely with the root mean square of the velocity fluctuations. This result could support the notion of Bewersdorff & Ohlendorf (1988) that drag-reduction is associated with the formation of aggregates of micelles of the order of 1 mm. Large-scale turbulence would be

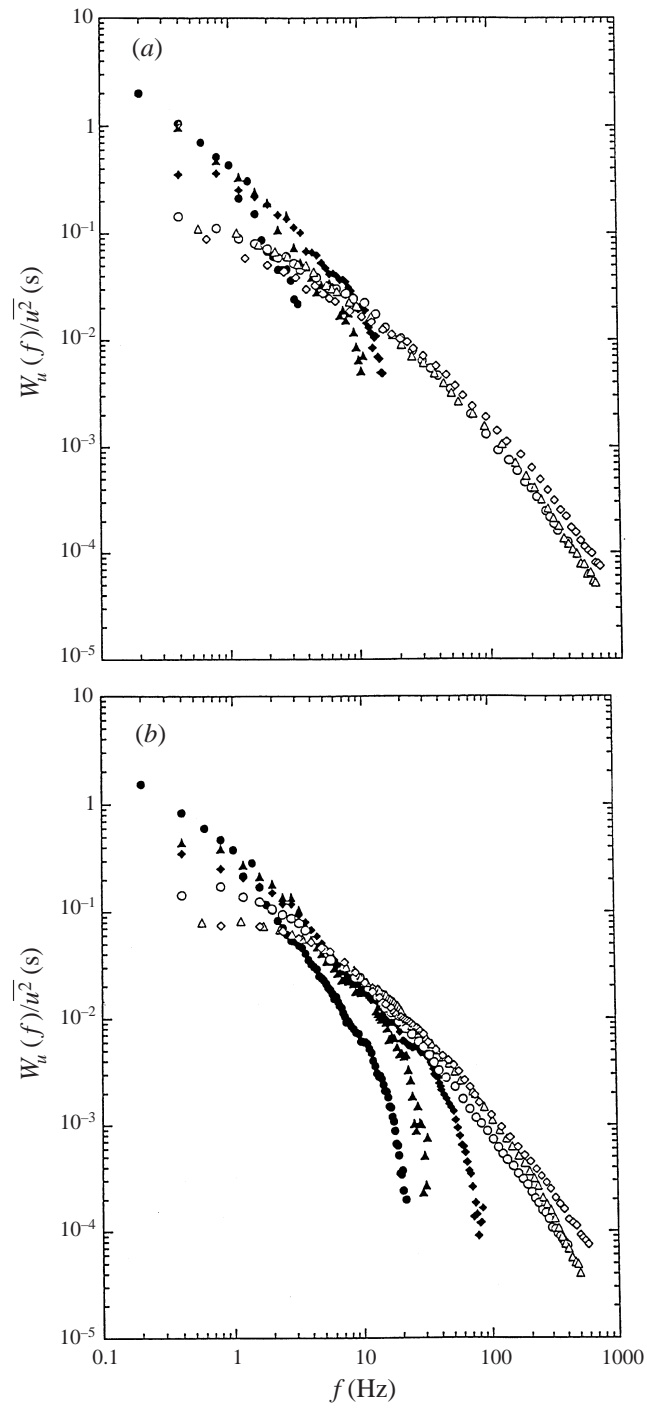


FIGURE 11(a, b). For caption see page 18.

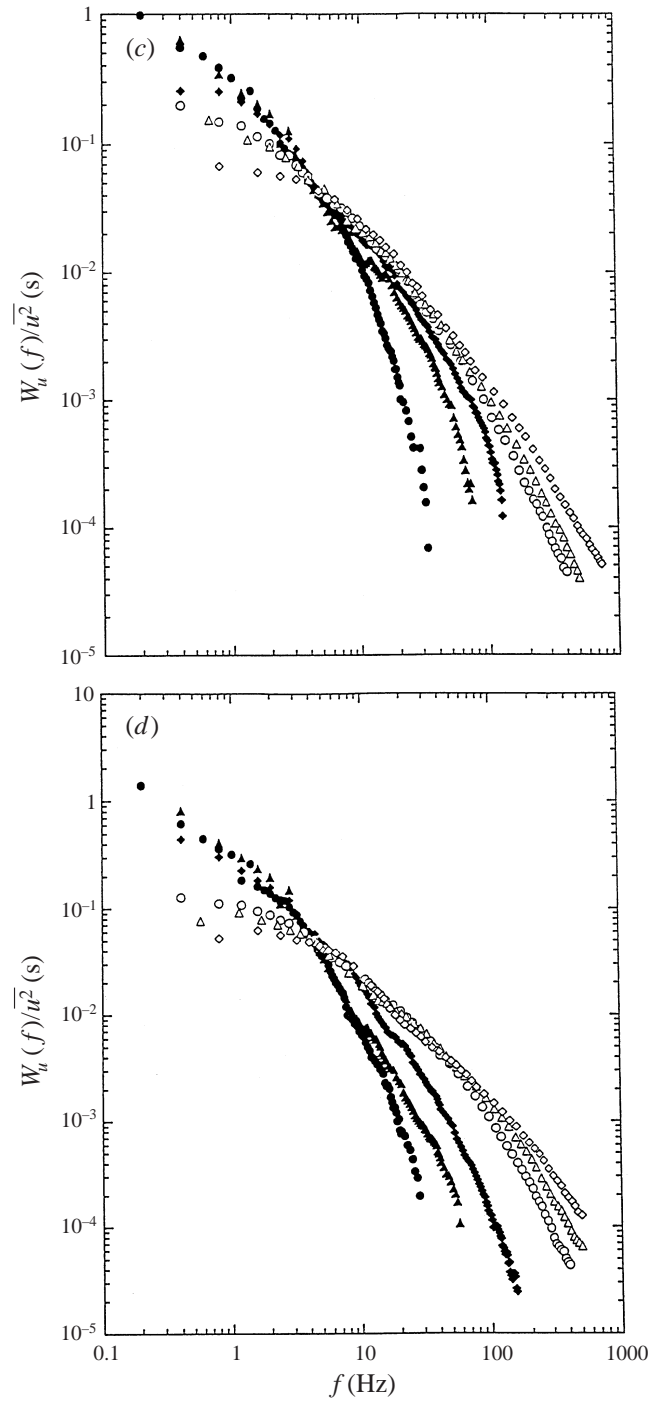


FIGURE 11. Streamwise velocity power spectra with the spectral density function normalized with the mean square of the velocity fluctuations, (a) at $y/H = 1.0$; (b) at $y/H = 0.6$; (c) at $y/H = 0.4$; (d) at $y/H = 0.1$. ET/13-50: \bullet , $Re = 19\,100$; \blacktriangle , $32\,000$; \blacklozenge , $49\,100$. Water: \circ , $Re = 20\,300$, \triangle , $31\,200$; \diamond , $48\,800$.

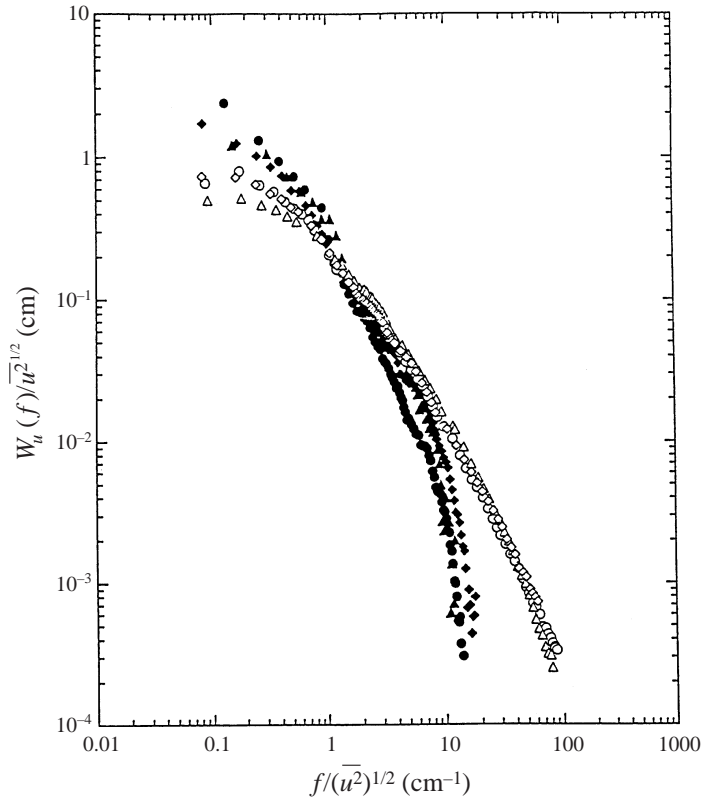


FIGURE 12. Streamwise velocity power spectra at $y/H = 0.6$ with the spectral density function and frequency normalized by the root mean square of the velocity fluctuations. ET/13-50: \bullet , $Re = 19\,100$; \blacktriangle , $32\,000$; \blacklozenge , $49\,100$. Water: \circ , $Re = 20\,300$, \triangle , $31\,200$; \diamond , $48\,800$.

created but velocity fluctuations with smaller scales than the structures could be dampened.

From the studies of Lui *et al.* (1996) we conclude that the micelles used in this study are threadlike and entangled. This could be a general feature of other drag-reducing systems that show very large drag-reduction, such as polymer solutions (Warholic 1997) and fibre suspensions (McComb & Chan 1985). All of these studies, both in circular pipes and in rectangular channels, show ‘maximum drag-reduction’ which is not a laminar flow. The few measurements of Reynolds shear stresses that are now becoming available indicate that they are close to zero for very large drag-reductions, such as are realized for maximum drag-reduction.

It is now known that, for Newtonian fluids, flow-oriented vortices are formed close to a wall by a reorganization of the vorticity generated at the wall. These vortices are essential in the development of Reynolds stresses. An attractive explanation for drag-reduction is that aggregates of long chainlike or threadlike additives interact with these vortices, particularly at their formation, in such a way that large positive values of $\tau_{ij}^m(\partial u_j / \partial x_i)$ are produced locally. This would result in a damping of the vortices; under maximum drag-reduction, the wall vortices do not exist. Thus, it might be more useful to compare the behaviour at maximum drag-reduction with a laminar flow than with a turbulent flow of a Newtonian fluid.

This work is being supported by the National Science Foundation through grant CTS-92-00936. The authors gratefully acknowledge the help provided by Professors J. L. Zakin and Dr C. F. Zuko Bin Liu and Mr William Hunt.

REFERENCES

- BEIERSDORFER, H., BEWERSDORFF, H.-W. & GYR, A. 1994 Flows with surfactant at maximum drag reduction. *Proc. IUTAM symp. on Liquid Particle Interactions in Suspension Flow, Grenoble*.
- BEWERSDORFF, H. W. 1990 Drag reduction in surfactant solutions. In *Structure of Turbulence and Drag Reduction* (ed. A. Gyr), pp. 293–212. Springer.
- BEWERSDORFF, H. W. & OHLENDORF, D. 1988 The behaviour of drag reducing cationic surfactant solutions. *Colloid Polymer Sci.* **266**, 941–953.
- CHARA, Z., ZAKIN, J. L., SEVERA, M. & MYSKA, J. 1993 Turbulence measurements of drag reducing surfactant systems. *Exps. Fluids* **16**, 36–41.
- GÜNTHER, A., PAPAVALASSIOU, D. V., WARHOLIC, M. D. & HANRATTY, T. J. 1998 Turbulent flow in a channel at a low Reynolds number. *Exps. Fluids* **25**, 503–511.
- GYR, A. & BEWERSDORFF, H.-W. 1995 *Drag Reduction of Turbulent Flows by Additives*. Kluwer.
- HOFFMAN, S., STERN, P. & MYSKA, J. 1994 Rheological behaviour and birefringence investigations on drag reducing surfactant solutions of tallow (trishydroxyethyl)-ammonium acetate/sodium salicylate mixtures. *Rheol. Acta* **33**, 419–430.
- KAWAGUCHI, Y., TAWARAYA, Y., YABE, A., HISHIDA, K. & MAEDA, M. 1996 Active control of turbulent drag reduction in surfactant solutions for wall heating. *Fluids Engng Div. Conf. ASME* **2**, 47–52.
- LUI, B., YESHAYAHU, T. & ZAKIN, J. L. 1996 Effect of counter ion to surfactant ratio on rheology and drag reduction behaviours of cationic surfactant solutions. *Fluids Engng Div. Conf. ASME*, **2**, 169–175.
- MCCOMB, W. D. & S. CHAN, K. T. J. 1985 Laser-Doppler anemometer measurements of turbulent structure in drag-reducing fibre suspensions. *J. Fluid Mech.* **152**, 455–478.
- MYSELS, K. J. 1949 Flow of thickened fluids. US Patent 2,492,173.
- NIEDERSCHULTE, M. A., ADRIAN, R. J. & HANRATTY, T. J. 1990 Measurements of turbulent flow in a channel at low Reynolds numbers. *Exps. Fluids* **9**, 222–231.
- OHLENDORF, D., INHERTHAL, W. & HOFFMAN, H. 1986 Surfactant systems for drag reduction: physico-chemical properties and rheological behaviour. *Rheol. Acta* **26**, 468–486.
- POVKH, I. L., STUPVI, A. V. & ASLANOV, P. V. 1988 Structure of turbulence in flows with surfactant and polymeric additives. *Sov. Res.* **17**, 65–79.
- SCHMIDT, G. M. 1997 Surfactant induced drag reduction in a channel flow facility. BS thesis, University of Illinois, Urbana.
- VIRK, P. S. & MICKLEY, H. S. 1970 The ultimate asymptote and mean flow structures in Toms' phenomenon. *Trans. ASME E: J. Appl. Mech.* **37**, 488–493.
- WARHOLIC, M. D. 1997 Drag reduction in turbulent channel flow by additives. PhD thesis, University of Illinois, Urbana.
- WHITE, A. 1967 Flow-characteristics of complex soap systems. *Nature* **214**, 585–586.
- ZAKIN, J. L. & LUI, H. L. 1983 Variables affecting drag reduction by nonionic surfactant additives. *Chem. Engng Commun.* **23**, 77–80.
- ZAKIN, J., MYSKA, J. & CHARA, Z. 1996 New limiting drag reduction and velocity profile asymptotes for nonpolymeric additives systems. *AIChE J.* **42**, 3544–3546.